CHAPTER 6

SIMULATION OF HYPERVELOCITY IMPACT EFFECTS ON REINFORCED CARBON-CARBON

Young-Keun Park[1] **and Eric P. Fahrenthold**[2]

Department of Mechanical Engineering, 1 University Station C2200
University of Texas, Austin, TX 78712, USA

[1]Graduate student

[2]Professor, corresponding author, phone: (512) 471-3064, email: epfahren@mail.utexas.edu

ABSTRACT

Spacecraft operating in low earth orbit face a significant orbital debris impact hazard. Of particular concern, in the case of the Space Shuttle, are impacts on critical components of the thermal protection system. Recent research has formulated a new material model of reinforced carbon-carbon, for use in the analysis of hypervelocity impact effects on the Space Shuttle wing leading edge. The material model has been validated in simulations of published impact experiments and applied to model orbital debris impacts at velocities beyond the range of current experimental methods. The results suggest that momentum scaling may be used to extrapolate the available experimental data base, in order to predict the size of wing leading edge perforations at impact velocities as high as 13 km/s.

NOMENCLATURE

d, shear damage variable	δ_{ij}, Kronecker delta
D, projectile diameter	$\mathbf{L}$, velocity gradient tensor
D_p, perforation diameter	$\mathbf{N}_e$, number of elements
D_c, coating spall diameter	$\mathbf{R}$, rotation matrix
$\mathbf{D}$, rate of deformation tensor	$\mathbf{S}$, deviatoric stress tensor
$\mathbf{e}$, Euler parameter vector	$\mathbf{S}^p$, effective stress tensor
$\overline{\mathbf{E}}$, deviatoric strain tensor	s, entropy density
$\mathbf{E}^e$, elastic strain tensor	v, impact velocity
$\mathbf{E}^p$, plastic strain tensor	Y, yield stress
ε^p, effective plastic strain	ψ, strain energy density
$\dot{\varepsilon}$, deviatoric strain rate	θ, temperature
$\mathbf{F}$, deformation gradient tensor	ϕ, impact obliquity

INTRODUCTION

Carbon-carbon composites offer an unusual combination of thermal and mechanical properties.[1] Their light weight and high temperature strength satisfy some very stringent design requirements for reusable orbital vehicles.[2] The wing leading edge of the Space Shuttle, subject to severe thermal re-entry loads, is constructed of reinforced carbon-carbon (RCC) panels, coated in silicon carbide to prevent oxidation.[3] Although the thermal properties of RCC composites are well understood,[4] much less is known about their dynamic mechanical properties. The loss of the Space Shuttle Columbia,[5] apparently due to impact damage on the wing leading edge, has motivated recent experimental[6] and computational[7] work aimed at developing a better understanding of the impact response of thermal protection materials.

The wing leading edge damage to Columbia was unexpected, the result of a relatively low velocity impact by a relatively low density projectile.[8] Another impact damage hazard, due to space debris in low earth orbit, has long been recognized. This threat involves projectiles of very low mass, but much higher density, and impact velocities as high 15 km/s. The debris shielding on the International Space Station is designed to defeat centimeter sized aluminum projectiles. Although the likelihood of such a projectile striking the Space Shuttle is quite low, orbital debris damage by much smaller projectiles is routinely observed during post-mission inspections of the vehicle. As a result previous experimental research has investigated the response of Space Shuttle thermal protection materials to orbital debris impact by spherical aluminum projectiles as large as 0.628 cm in diameter.[9]

Due to the high cost of carbon-carbon composites and the long fabrication lead times associated with the preparation of test samples, impact testing of RCC materials has been limited. In addition, the limitations of current experimental technology preclude hypervelocity impact testing over the entire projectile mass and kinetic energy range of interest. As a result, numerical simulation can serve as an important complement to experimental studies of the impact response of RCC materials. Numerical models validated by comparison with

experiment at velocities below 8 km/s can be used to extrapolate results into a higher velocity impact regime. A coordinated experimental and computational approach to the study of RCC response to insulating foam impacts has proven to be productive;[10] the present paper extends the latter computational work, to projectiles and impact velocities associated with orbital debris impact. In particular it develops a new anisotropic, rate-dependent material model for reinforced carbon-carbon, validates that model in three dimensional simulations of published hypervelocity impact experiments, and applies the validated formulation in simulations of impacts at velocities beyond the experimental range. The results indicate that a momentum scaling approach used to correlate the available experimental impact data may be extrapolated to describe RCC perforation by hypervelocity projectiles at velocities as high as 13 km/s.

The present paper is organized as follows. The first section outlines the hybrid particle-finite element method used in the present study, including the imbedded large deformation kinematics and general functional forms for the associated constitutive relations. The second section discusses published experimental results on the properties of RCC. The third section develops an RCC constitutive model, formulated for use in hypervelocity impact applications and reflecting important mechanical characteristics described in the material testing literature. The fourth section validates and applies the developed model in a series of three dimensional impact simulations. The last section presents conclusions and suggestions for related future work.

NUMERICAL METHOD

The material model described in this paper was developed for application in a specific numerical framework, the hybrid particle-finite element formulation of references 11 and 12. In order to provide appropriate context, this section summarizes the latter numerical formulation, details certain element level kinematics, and provides functional forms for the

required constitutive relations. The kinematic and constitutive modeling framework assumed here has wide scope, so that the material model described in the present paper may be adapted for use in shock physics codes which are based on alternative numerical modeling schemes.[13]

The hybrid particle-finite element model employed here takes an explicit state space form. The state equations consist of evolution equations for the following variables:

- translational and rotational momentum vectors for the three dimensional motion of ellipsoidal particles,
- center of mass position vectors and Euler parameters for the particles, the latter providing a singularity free description of particle rotations,
- density and entropy for each particle, and
- damage and plastic internal state variables for each finite element.

The state equations are derived using a thermomechanical formulation of the Lagrange equations. All inertia effects are modeled using the particles, whose mass centers are also nodal coordinates for the finite elements. The volumetric thermomechanical response of the modeled medium is described by an equation of state for the particles, which may take either an analytic or tabular form.

The material modeling work described in the present paper develops two specific components of the general numerical formulation:

- a strain energy density in shear, one part of the thermomechanical Lagrangian for the modeled particle-element system, and
- a plasticity model which specifies evolution equations for the plastic internal state variables, equations which serve as nonholonomic constraints on the system level model.

The strain energy density in shear takes the general functional form

$$\psi \;=\; \psi(d, \mathbf{e}, \overline{\mathbf{E}}, \mathbf{E}^p) \tag{1}$$

where d is a shear damage variable, $\overline{\mathbf{E}}$ is the total deviatoric strain, $\mathbf{E}^p$ is the plastic strain, and $\mathbf{e}$ is a vector of Euler parameters which relates a material reference frame for each element to a single global Cartesian reference frame. The evolution equations for the plastic strain components take the general functional form

$$\dot{\mathbf{E}}^p \;=\; \dot{\mathbf{E}}^p(s, d, \varepsilon^p, \dot{\varepsilon}, J, \mathbf{e}, \overline{\mathbf{E}}, \mathbf{E}^p) \tag{2}$$

where s is an entropy density, ε^p is the effective plastic strain, $\dot{\varepsilon}$ is a deviatoric strain rate, and

$$J = det(\mathbf{F}) \tag{3}$$

where $\mathbf{F}$ is the deformation gradient tensor.

The strain and strain rate variables which appear in the preceding functional forms are defined by the following large deformation kinematics.[14] The deviatoric strain is

$$\overline{\mathbf{E}} = \frac{1}{2}\left(\,\overline{\mathbf{C}} - \mathbf{I}\,\right) \tag{4}$$

where

$$\overline{\mathbf{C}} = \overline{\mathbf{F}}^T\overline{\mathbf{F}}, \qquad \overline{\mathbf{F}} = (det\,\mathbf{F})^{-\frac{1}{3}}\,\mathbf{F} \tag{5}$$

The elastic shear strain is defined as

$$\mathbf{E}^e = \overline{\mathbf{E}} - \mathbf{E}^p \tag{6}$$

where the flow rule for the plastic stain tensor must satisfy the isochoric plastic deformation constraint

$$tr\left(\mathbf{C}^{p-T}\dot{\mathbf{C}}^p\right) = 0, \qquad \mathbf{C}^p = \mathbf{I} + 2\,\mathbf{E}^p \tag{7}$$

The effective plastic strain is determined by integrating the rate relation

$$\dot{\varepsilon^p} = ||\dot{\mathbf{E}}^p|| \tag{8}$$

with the indicated invariant operator defined by

$$||\mathbf{T}|| = \left[\frac{1}{2}\, tr\left(\mathbf{T}^T\mathbf{T}\right)\right]^{1/2} \tag{9}$$

for any second order tensor $\mathbf{T}$. The deviatoric strain rate is

$$\dot{\varepsilon} = ||\mathbf{D}'||, \qquad \mathbf{D}' = \mathbf{D} - \frac{1}{3} tr(\mathbf{D})\, \mathbf{I} \tag{10}$$

where $\mathbf{D}$ is the rate of deformation tensor

$$\mathbf{D} = \frac{1}{2}\left(\mathbf{L} + \mathbf{L}^T\right), \qquad \mathbf{L} = \dot{\mathbf{F}}\, \mathbf{F}^{-1} \tag{11}$$

with $\mathbf{L}$ the velocity gradient tensor.

In the case of anisotropic materials, the constitutive response is described in a material reference frame. Here an Euler parameter vector

$$\mathbf{e} = [e_0\, e_1\, e_2\, e_3]^T, \qquad \mathbf{e}^T\mathbf{e} = 1 \tag{12}$$

is used to define a rotation matrix ($\mathbf{R}$) for each element

$$\mathbf{R} = \mathbf{A}\, \mathbf{G}^T \tag{13}$$

$$\mathbf{A} = \begin{bmatrix} -e_1 & e_0 & -e_3 & e_2 \\ -e_2 & e_3 & e_0 & -e_1 \\ -e_3 & -e_2 & e_1 & e_0 \end{bmatrix} \tag{14}$$

$$\mathbf{G} = \begin{bmatrix} -e_1 & e_0 & e_3 & -e_2 \\ -e_2 & -e_3 & e_0 & e_1 \\ -e_3 & e_2 & -e_1 & e_0 \end{bmatrix} \tag{15}$$

which relates a material reference frame in each element to the global Cartesian system used in the numerical simulations. The rotation matrix relates vector components $\mathbf{p}$ in the global

coordinate system to corresponding components $\mathbf{q}$ described in the material reference frame, using

$$\mathbf{p} = \mathbf{R}\,\mathbf{q} \tag{16}$$

The corresponding transformation relation for second order tensors is

$$\mathbf{P} = \mathbf{R}\,\mathbf{Q}\,\mathbf{R}^T \tag{17}$$

where the components $\mathbf{P}$ refer to the global frame and the components $\mathbf{Q}$ refer to the material reference frame.

REINFORCED CARBON-CARBON

The published material property data base for carbon-carbon composites is limited by material costs and proprietary considerations. On the other hand, the complex nature of both the material and the application of interest here means that a rather wide range of experiments are needed to fully characterize its constitutive response. This section discusses some properties of RCC of particular significance in hypervelocity impact applications.

The most directly relevant experimental results are those of Lu et al.,[6] who performed tests at Sandia National Laboratories on samples taken from Space Shuttle wing leading edge panels, in support of the Columbia accident investigation. They provide data on elastic moduli as well as strength measurements obtained from tension, bending, and compression tests. Although the elastic moduli measured in tension and compression were similar, strength in compression was approximately double that in tension. In addition they reported a strain rate dependence of the tensile strength, observing a fifteen percent increase in strength as the loading rate increased from 1 to 200 sec^{-1}. Finally they noted that removal of the silicon carbide coating from the tested samples showed little effect on the measured mechanical properties.

Several different authors have reported results of shear tests performed on carbon-carbon composites.[15−20] In the case of the RCC, interlaminar shear strength and stiffness is of interest, since oblique hypervelocity impacts will in general lead to multi-axial loading. The published shear test data show that interlaminar shear stiffness and strength can differ by factors of approximately two and four respectively, from their in-plane counterparts.

Perhaps the most unusual property of RCC is its increase in strength with temperature,[17,21] by as much as a factor of two, as compared to the thermal softening response observed in metals. The high temperature strength of RCC is important in hypervelocity impact applications, due to the adiabatic heating typically associated with shock loading.

The preceding references, along with the equation of state literature[22] and published data on the thermal properties of RCC,[4,23] were used to estimate the material parameters used in the simulations reported in a later section. Although additional tests on Space Shuttle wing leading edge panels, like those reported by Lu at al., are needed, the cited references represent the best data available to the authors at the time the simulations were conducted.

MATERIAL MODEL

Composite materials are used in structural,[24] orbital debris shielding,[25] and thermal protection[4] applications on a variety of spacecraft, hence their response to hypervelocity impact effects has been analyzed in a number of previous experimental[26] and computational[27] studies. Previous material modeling work has considered both micromechanical[28] and anisotropic continuum models. The present paper employs an anisotropic continuum approach, since the high computational cost of micromechanical models normally precludes their use in structural scale simulations. Large deformation, anisotropic continuum models of composite materials[29,30] normally address shock physics problems by extending small strain formulations originally developed for applications in structural mechanics. In an alternative approach, the present work starts with the finite strain, hybrid particle-element kinematics

discussed in an earlier section, and then formulates: (1) an anisotropic strain energy density function which depends on a general deviatoric Lagrangian strain tensor, and (2) an anisotropic, temperature and rate dependent plastic flow rule which depends on an effective stress[31] and satisfies a general isochoric deformation constraint. Both the strain energy density function and the plastic flow rule: (1) account for differences in material response under tension and compression, (2) account for material reference frame dependence under large deformations, and (3) satisfy first and second law thermodynamic constraints. The approach used here has been applied with success to model isotropic materials.[32] It is motivated by a focus on hypervelocity problems, where large deformation dynamics are of central interest, and by the kinematic form of the hybrid numerical method used in the present paper. As indicated in the later section on simulations, this material modeling approach provides an accurate description of hypervelocity impact effects in reinforced carbon-carbon. Potential application of the formulation to model impact in other composites, such as graphite-epoxy or Kevlar-epoxy, is of interest for future work.

In the case of an orthotropic material, with distinct elastic moduli in tension and compression, the shear strain energy density per unit reference volume is

$$\begin{aligned} \psi &= (1-d)\,\mu_o\,\frac{1}{2}\sum_{i=1}^{3}\mu_{ii}\left[(1+\gamma_i)+(1-\gamma_i)\,sgn(E^{em}_{ii})\right](E^{em}_{ii})^2 + \\ &\quad (1-d)\,\mu_o\sum_{i=1}^{3}\sum_{j=1}^{3}(1-\delta_{ij})\,\mu_{ij}\,(E^{em}_{ij})^2 \end{aligned} \tag{18}$$

where δ_{ij} is the Kronecker delta, μ_o is a reference elastic modulus, and the parameters $\mu_{ij} = \mu_{ji}$ are dimensionless constants. The parameters γ_i are the ratios of the elastic moduli in compression to those in tension, while the E^{em}_{ij} are the components of the elastic shearing strain, expressed in a material reference frame. Note that this function is analytic, since a change in modulus from tension to compression occurs when the corresponding material strain component is zero.

A plastic flow rule for an anisotropic, rate dependent material, which satisfies the afore-

mentioned isochoric plastic deformation constraint, may be obtained by extending a large strain Lagrangian formulation previously developed for use in hypervelocity impact applications.[32,33] The flow rule is

$$\dot{\mathbf{E}}^p = \frac{\dot{\lambda}}{||\mathbf{S}^p||} \underline{\underline{\mathbf{N}}}^p \, \underline{\underline{\mathbf{N}}} \, \underline{\underline{\mathbf{M}}} \, \underline{\underline{\mathbf{M}}}^p \, \mathbf{S}^p \tag{19}$$

where $\dot{\lambda}$ is a positive proportionality coefficient, $\mathbf{S}^p$ is the effective stress,

$$\mathbf{S}^p = \underline{\underline{\mathbf{M}}}^{pT} \, \underline{\underline{\mathbf{M}}}^T \, \underline{\underline{\mathbf{N}}}^T \, \underline{\underline{\mathbf{N}}}^{pT} \, \mathbf{S} \tag{20}$$

and $\mathbf{S}$ is the deviatoric stress tensor

$$\mathbf{S} = \frac{\partial \psi}{\partial \mathbf{E}^e} \tag{21}$$

The first two coefficients in the flow rule impose the isochoric plastic deformation constraint, and are defined by

$$\underline{\underline{\mathbf{N}}}^p \, \mathbf{T} = \frac{1}{2 \, ||\mathbf{C}^p||} (\mathbf{C}^p \, \mathbf{T} + \mathbf{T} \, \mathbf{C}^p) \tag{22}$$

and

$$\underline{\underline{\mathbf{N}}} \, \mathbf{T} = \mathbf{T} - \frac{1}{3} tr(\mathbf{T}) \, \mathbf{I} \tag{23}$$

for any symmetric second order tensor $\mathbf{T}$. The third coefficient performs a component transformation from a material reference frame to a fixed global frame, and is defined by

$$\underline{\underline{\mathbf{M}}}^T \, \mathbf{T} = \mathbf{R}^T \, \mathbf{T} \, \mathbf{R} \tag{24}$$

for any symmetric second order tensor $\mathbf{T}$. The last coefficient in the flow rule defines an effective stress transformation, in a material reference frame, using

$$\underline{\underline{\mathbf{M}}}^{pT} \, \mathbf{P} = \mathbf{Q} \tag{25}$$

for symmetric second order tensors $\mathbf{P}$ and $\mathbf{Q}$, with component forms

$$Q_{ii} = \frac{2 \, \alpha_{ii} \, P_{ii}}{(1 + \beta_{ii}) + (1 - \beta_{ii}) \, sgn(E^{em}_{ii})} \quad , \qquad i = 1, 2, 3 \tag{26}$$

and

$$Q_{ij} = \frac{2\,\alpha_{ij}\,P_{ij}}{(1+\beta_{ij}) + (1-\beta_{ij})\;sgn(J-1)} \quad , \qquad i \neq j \tag{27}$$

The parameter $\alpha_{ij} = \alpha_{ji}$ is the ratio of a reference yield stress to the yield stress for the ijth stress component, while the parameter $\beta_{ij} = \beta_{ji}$ is the ratio of the strength in compression to that in tension for the ijth stress component.

The rate dependent, strain hardening, thermal softening yield function is

$$f = ||\mathbf{S}^p|| - Y \tag{28}$$

where Y is the yield stress

$$Y = \frac{1}{2}\,(1-d)\,Y_o\,\left(1-\kappa\,\theta^H\right)\,(1+\eta\,\varepsilon^p)^n\,\left[1+\zeta\;log\left(\frac{\dot{\varepsilon}}{\dot{\varepsilon}_o}\right)\right]^m \tag{29}$$

with Y_o the reference yield stress, η a strain hardening coefficient, n a strain hardening exponent, ζ a strain rate hardening coefficient, m a strain rate hardening exponent, $\dot{\varepsilon}_o$ a reference strain rate, κ a thermal softening coefficient, and θ^H the homologous temperature

$$\theta^H = \frac{\theta - \theta_o}{\theta_m - \theta_o} \tag{30}$$

where θ_o and θ_m are reference and melt temperatures.

In a numerical implementation, the aforementioned plastic flow rule is expressed in incremental form. That is the incremental plastic strain at each time step is computed using the incremental proportionality coefficient

$$\Delta\lambda = max\left(0\,,\,\frac{||\mathbf{S}^p|| - Y}{(1-d)\,2\,\mu_o}\right) \tag{31}$$

The shear damage variable (d) models the transition from an intact to a failed medium, evolving from an initial value of 0 to a final value of 1 over a fixed number of time steps[34] when any stipulated element failure criterion is satisfied. The simulations discussed in the next section incorporate accumulated plastic strain, melt temperature, and maximum compression failure criteria, although other criteria may be accommodated.

IMPACT SIMULATIONS

The material model just described was applied in a series of three dimensional simulations of hypervelocity impacts on reinforced carbon-carbon. The simulations employed a hybrid particle-finite element method and the material properties listed in Tables 1 and 2. An initial set of simulations was used to validate the material model, compare results obtained using analytic (Mie Gruneisen) and tabular[35] (SESAME 3715) equations of state, and check numerical convergence of the simulation results. A second series of simulations was then performed to estimate orbital debris impact effects at velocities beyond the range of current experimental methods.

The first set of eight simulations modeled NASA JSC experiments B1028 and B1040,[9] which involved oblique impacts of aluminum spheres on reinforced carbon-carbon target plates at a velocity of seven kilometers per second. The target plates were 0.63 cm in thickness, including upper and lower surface coatings composed of silicon carbide, each 0.08 cm in thickness. Table 3 lists the simulation parameters, including projectile diameter (D), impact velocity (v), impact obliquity (ϕ, with zero degrees a normal impact), number of elements spanning the target thickness (N_e), and the equation of state used to model the aluminum projectile. Tabular equation of state data was not available for the target materials.

Figures 1 through 4 show example plots for a simulation of experiment B1028. Figure 1 shows the initial configuration while Figures 2 through 4 show the simulation results at 50 microseconds after impact. The sectioned plot in Figure 4 depicts plate perforation and coating spall similar to that observed in the corresponding experiment. Table 3 lists simulation results for the diameter of the RCC perforation (D_p) and the average diameter of the target region over which the silicon carbide coating was removed (D_c). The results of the validation simulations suggest the following conclusions:

- the material model developed here can provide good estimates of both the RCC perforation diameter and the extent of the spalled coating region, for oblique impacts at seven kilometers per second,
- accurate estimates of the RCC perforation diameter require a mesh resolution sufficient to place 8 elements across the target plate,
- accurate estimates of the diameter of the spalled coating region require a mesh resolution sufficient to place 16 elements across the target plate, and
- the simulation results are not sensitive to the choice of projectile equation of state.

Table 4 shows the relative computational cost of simulations of experiments B1028 and B1040 run at three different mesh densities. As is well known, in three dimensional models the particle count increases with the cube of the increase in resolution, while the time step decreases linearly with the increase in resolution, so that the total computational cost of high resolution models is considerable.

A second set of twelve simulations was performed to investigate orbital debris impact effects at velocities beyond the current experimental range. The simulations involved spherical aluminum projectiles, at three different projectile diameters, an impact obliquity of 30 degrees and impact velocities of 7, 10, and 13 km/s. In the case of the largest projectile, simulations were performed using both an analytic and a tabular equation of state. The target assumed in these simulations was identical to that involved in the aforementioned experiments. In the target mesh 8 elements spanned the plate thickness, so that the resolution level was sufficient to estimate the diameter of the RCC perforations, but not the extent of the region of coating spall. Figure 5 shows simulation results for the diameters of the RCC perforations, as a function of projectile diameter, impact velocity, and projectile equation of state. In Figure 5, MG denotes the Mie Gruneisen analytic equation of state, while SES

denotes the SESAME tabular equation of state. The results of these simulations suggest the following conclusions, for the impact velocity range and impact obliquity considered:

- perforation diameters increase with both projectile size and impact velocity, over the full range of the simulations,
- for a fixed projectile size, perforation diameters increase with impact velocity at an approximately linear rate,
- for a fixed impact velocity, perforation diameters increase with projectile size, but at a declining rate, and
- the simulation results are not sensitive to the choice of projectile equation of state.

Note that Figure 5 is not a ballistic limit plot; rather it plots perforation diameter versus impact velocity, so that the indicated trends are not unexpected.

Although the preceding results are informative, they consider only a limited rage of projectile size and obliquity. Hence the scaling of the simulation results, as compared to the available experimental data, is of considerable interest. Figure 6 shows a plot of perforation diameter versus normal impact momentum for the 11 different projectile size and impact velocity combinations modeled in the present computational study, as well as corresponding data for 15 published experiments.[9,36] The experiments involved projectile diameters ranging from 0.039 to 0.628 cm, impact velocities ranging from 2.49 to 7.32 km/s, and impact obliquities ranging from 0 to 80 degrees. The simulations involved a more limited range of projectile diameters (0.123 to 0.360 cm) and obliquities (30 to 45 degrees), but a much higher range of impact velocities (7 to 13 km/s). All of the simulations and experiments of course involved the same target configuration. The data in Figure 6 suggests that the experimental and simulation results for the diameters of RCC perforations scale with normal impact momentum in a similar fashion. Although these results do not establish a universal

scaling relation for the problem of interest, they do suggest that the scaling of perforation size with normal impact momentum observed in experiments below 8 km/s may be extrapolated to much of the velocity range of interest in orbital debris impact applications.

CONCLUSION

The present paper has formulated an anisotropic, rate dependent material model for use in the simulation of hypervelocity impact problems. The material model was developed to study orbital debris impact effects on reinforced carbon-carbon materials, and has been validated in simulations of hypervelocity impact experiments conducted at 7 km/s. The validated model was applied to simulate impacts at velocities beyond the experimental range. The results indicate that momentum scaling analysis, used to correlate a wide range of experiments below 8 km/s, has application in predicting perforation diameters for reinforced carbon-carbon targets at velocities as high as 13 km/s. The ability of reinforced carbon-carbon to retain its strength at high temperatures suggests that accurate strength models of this material are important in simulations of impact effects over the entire orbital debris velocity range.

Some conclusions relevant to future work are suggested:

- additional high resolution simulations are needed in order to investigate the spallation of silicon carbide coating at velocities above the current experimental range,
- additional mechanical properties testing is needed, at elevated temperatures and high strain rates, to support the development and validation of improved strength models for reinforced carbon-carbon,
- additional equation of state research is needed, to provide tabular data applicable to reinforced carbon-carbon materials over a wide range of impact velocities, and

- the development of advanced thermal protection materials should in the future include experimental work aimed at detailed characterization of their mechanical as well as their thermal properties.

The use of composite materials in spacecraft applications complicates both experimental and computational studies of impact effects. High cost materials with long fabrication lead times, such as reinforced carbon-carbon, and the limitations of current experimental impact techniques motivate the increased use of computer simulation in the design of spacecraft for micrometeoroid and orbital debris impact effects.

Acknowledgments — This work was supported by NASA Johnson Space Center (NAG 9-1244) and by the National Science Foundation (CMS 99-12475). Computer time support was provided by the Texas Advanced Computing Center at the University of Texas at Austin and the Arctic Region Supercomputing Center at the University of Alaska Fairbanks.

REFERENCES

1. T. Windhorst and G. Blount, 1997, "Carbon-Carbon Composites: a Summary of Recent Developments and Applications," Materials and Design, volume 18, Number 1, pp. 11-15.

2. D.L. Schmidt, K.E. Davidson and L.S. Theibert, 1999, "Unique Applications of Carbon-Carbon Composite Materials (Part One)," SAMPE Journal, Volume 35, pp. 27-39.

3. G. Savage, 1993, "Carbon-Carbon Composites," Chapman and Hall, London.

4. C.W. Ohlhorst, W.J. Vaughn, P.O. Ransone, and H.T. Tsou, 1997, "Thermal Conductivity Database of Various Structural Carbon-Carbon Composite Materials," NASA TM 1997-4787.

5. Report of the Columbia Accident Investigation Board, Volume 1, Government Prining Office, Washington, DC, August 2003.

6. W.-Y. Lu, B.R. Antoun, J.S. Korellis, S. Scheffel, M.Y. Lee, R.D. Hardy, and L.S. Costin, "Material Characterization of Shuttle Thermal Protection System for Impact Analyses," AIAA-2004-0945, presented at the 2004 AIAA Aerospace Sciences Meeting, Reno, Nevada, January 5-8,2004.

7. K.W. Gwinn and K.E. Metzinger, "Analysis of Foam Impact Onto the Columbia Shuttle Wing Leading Edge Panels Using Pronto3D/SPH," AIAA-2004-0942, presented at the 2004 AIAA Aerospace Sciences Meeting, Reno, Nevada, January 5-8,2004.

8. J.H. Kerr, D.J. Grosch, and E.L. Christiansen, "Impact Testing of Large Foam Projectiles," AIAA-2004-0939, presented at the 2004 AIAA Aerospace Sciences Meeting, Reno, Nevada, January 5-8,2004.

9. E.L. Christiansen and L. Friesen, 1997, "Penetration Equations for Thermal Protection Materials," International Journal of Impact Engineering, Volume 20, pp. 153-164.

10. Fahrenthold, EP, and Park, YK. "Simulation of foam impact effects on the space shuttle thermal protection system.," AIAA Journal of Spacecraft and Rockets, in press.

11. Fahrenthold, E.P., and Horban, B.A., 2001, "An improved hybrid particle-finite element method for hypervelocity impact simulation," International Journal of Impact Engineering, Vol. 26, pp. 169-178.

12. Shivarama, R., and Fahrenthold, E.P., 2004, "An ellipsoidal particle-finite element method for hypervelocity impact simulation," International Journal for Numerical Methods in Engineering, Volume 59, pp. 737-753.

13. J.M. McGlaun, S.L. Thompson, and M.G. Elrick, 1990, "CTH: A three dimensional shock wave physics code," International Journal of Impact Engineering, Volume 10, pp. 351-360.

14. L.E. Malvern, 1969, Introduction to the Mechanics of a Continuous Medium, Prentice Hall, Englewood Cliffs, New Jersey.

15. M.S. Aly-Hassan, H. Hatta, S. Wakayama, M. Watanabe and K. Miyagawa, 2003, "Comparison of 2D and 3D Carbon/Carbon Composites with respect to Damage and Fracture Resistance," Carbon, Volume 41, pp. 1069-1078.

16. K. Anand, V. Gupta and D. Dartford, 1994, "Failure Mechanisms of Laminated Carbon-Carbon Composites - II. Under Shear Loads," Acta metallurgica et materialia, volume 42, Number 3, pp.797-809.

17. E. Fitzer and L.M. Manocha, 1998, "Carbon Reinforcements and Carbon/Carbon Composites," Springer-Verlag, Berlin, Heidelberg, New York.

18. F. Abali, A. Pora and K. Shivakumar, 2003, "Modified Short Beam Shear Test for Measurement of Interlaminar Sheear Strength of Composites," Journal of Composite Materials, Volume 37, Number 5, pp.453-464.

19. C.G. Papakonstantinou, P. Balaguru and R.E. Lyon, 2001, "Comparative Study of High Temperature Composites," Composites: Part B, Volume 32, pp. 637-649.

20. L.C. Edgar, B. David and K.F. Mattison, 1996, "The Interlaminar tensile and Shear Behavior of a Unidirectional C-C Composite," Journal of Nuclear Materials, Volume 230, pp.226-232.

21. J.D. Buckley and D.D. Edie, 1993, "Carbon-Carbon Materials and Composites," Noyes Publications, New Jersey.

22. Steinberg DJ. Equation of State and Strength Properties of Selected Materials, 1996, Lawrence Livermore National Laboratory, UCRL-MA-106439.

23. K.J. Dowding, J.V. Beck and B.F. Blackwell, 1996, "Estimation of Directional-Dependent Thermal Properties in a Carbon-Carbon Composite," International Journal of Heat Mass Transfer, Volume 39, Number 15, pp. 3157-3164.

24. Christiansen, E.L., 1990, "Investigation of Hypervelocity Impact Damage to Space Station Truss Tubes," International Journal of Impact Engineering, Volume 10, pp. 125-133.

25. Destefanis, R., and Faraud, M., 1997, "Testing of Advanced Materials for High Resistance Debris Shielding," International Journal of Impact Engineering, Volume 20, pp. 209-222.

26. Yew, C.H., and Kendrick, R.B., 1987, "A Study of Damage in Composite Panels Produced by Hypervelocity Impact," International Journal of Impact Engineering, Volume 5, pp. 792-738.

27. Palmieri, D., Destefanis, R., Faraud, M., and Lambert, M., 2003, "Penetration Effectiveness of Inhibited Shaped Charge Launcher Projectiles and Solid Spheres on Spacecraft Shields," International Journal of Impact Engineering, Volume 29, pp. 513-526.

28. Silling SA, Taylor, PA, Wise, JL, and Furnish, MD. Micromechanical Modeling of Advanced Materials, 1994, SAND94-0129, Sandia National Laboratories.

29. Logan, RW. Incorporating Non-quadratic and Crystallographic Yields Surfaces in Finite Element Codes, 1988, LA-CP-88-186, Los Alamos National Laboratory, Los Alamos, New Mexico.

30. Hayhurst, CJ, Livingstone, IHG, Clegg, RA, Destefanis, R, and Faraud, M, 2001,"Ballistic Limit Evaluation of Advanced Shielding Using Numerical Simulations," International Journal of Impact Engineering, Volume 26, pp. 309-320.

31. Hill, R. The mathematical theory of plasticity, 1950, Oxford University Press.

32. Fahrenthold EP, Horban BA. , 1997, "Thermodynamics of continuum damage and fragmentation models for hypervelocity impact, " International Journal of Impact Engineering, Volume 20, pp. 241-252.

33. E.P. Fahrenthold and Y.K. Park, "Simulation of hypervelocity impact on aluminum-Nextel-Kevlar orbital debris shields," International Journal of Impact Engineering, Volume 29, 2003, pp. 227-235.

34. Silling SA. CTH Reference Manual: Johnson-Holmquist Ceramic Model, 1992, SAND92-0576, Sandia National Laboratories.

35. Lyon SP, Johnson JD, editors. SESAME: The Los Alamos National Laboratory Equation of State Database, LA-UR-92-3407, Los Alamos National Laboratory, Los Alamos, New Mexico.

36. F. Lyons, E.L. Christiansen, and J.H. Kerr. Hypervelocity Impact Testing of Reinforced Carbon-Carbon Composites, May 1998, Report JSC 23898, NASA Johnson Space Center.

Table 1. Material properties

Material property	Aluminum	Silicon Carbide	RCC
Reference bulk modulus ($Mbar$)	0.784	2.21	0.0576
Reference shear modulus ($Mbar$)	0.271	0.240	0.0718
Reference soundspeed ($cm\,\mu sec^{-1}$)	0.539	0.829	0.191
Mie-Gruneisen gamma	1.97	0.95	0.24
Mie-Gruneisen slope	1.34	1.21	1.33
Reference density ($g\,cm^{-3}$)	2.70	3.21	1.58
Reference yield stress ($kbar$)	2.90	0.771	0.771
Specific heat ($bar\,cm^3\,g^{-1}\,^\circ K^{-1}$)	8.84	7.12	7.12
Strain hardening coefficient	125	10	2
Strain hardening exponent	0.1	1.0	1.0
Strain rate hardening coefficient	0.0	0.0	0.1
Strain rate hardening exponent	0.0	0.0	1.0
Reference strain rate (sec^{-1})	0	0	0.01
Thermal softening coefficient	0.567	0.0	-1.0
Melt temperature ($^\circ K$)	1,220	3,840	3,840
Maximum compression	100	100	100
Plastic failure strain	1.00	0.10	0.50

Table 2. Material model parameters

Parameters	Silicon Carbide	Reinforced carbon-carbon
$\gamma_1 = \gamma_2 = \gamma_3$	0.10	1.00
$\mu_{11} = \mu_{22} = \mu_{33} = \mu_{13}$	1.00	1.00
$\mu_{12} = \mu_{23}$	1.00	0.50
$\alpha_{11} = \alpha_{22} = \alpha_{33} = \alpha_{13}$	1.00	1.00
$\alpha_{12} = \alpha_{23}$	1.00	3.73
$\beta_{11} = \beta_{22} = \beta_{33}$	2.00	2.00
$\beta_{12} = \beta_{13} = \beta_{23}$	2.00	2.00

Table 3. Numerical results, simulations of NASA JSC experiments B1028 and B1040

Test number	D (cm)	v (km/s)	ϕ (deg)	N_e	Equation of state	D_p (cm)	Error (%)	D_c (cm)	Error (%)
B1028	0.628	7.01	45	8	Mie Gruneisen	2.60	10.3	3.74	15.0
				8	SESAME 3715	2.65	8.6	3.60	18.2
				16	Mie Gruneisen	2.66	8.3	4.05	8.0
				24	Mie Gruneisen	2.67	7.9	4.08	7.3
B1040	0.478	6.96	30	8	Mie Gruneisen	2.12	3.6	2.95	21.3
				8	SESAME 3715	1.97	10.5	2.95	21.3
				16	Mie Gruneisen	2.00	10.0	3.38	9.9
				24	Mie Gruneisen	2.10	4.5	3.48	7.2

Table 4. Computer resource requirements, simulations of NASA JSC experiments

Test number	N_e	Total particles (million)	Total elements (million)	Number of processors	Wall clock hours
B1028	8	0.078	0.036	16	14
	16	0.572	0.275	64	65
	24	1.857	0.905	64	340
B1040	8	0.078	0.036	32	5
	16	0.572	0.275	64	74
	24	1.856	0.905	64	347

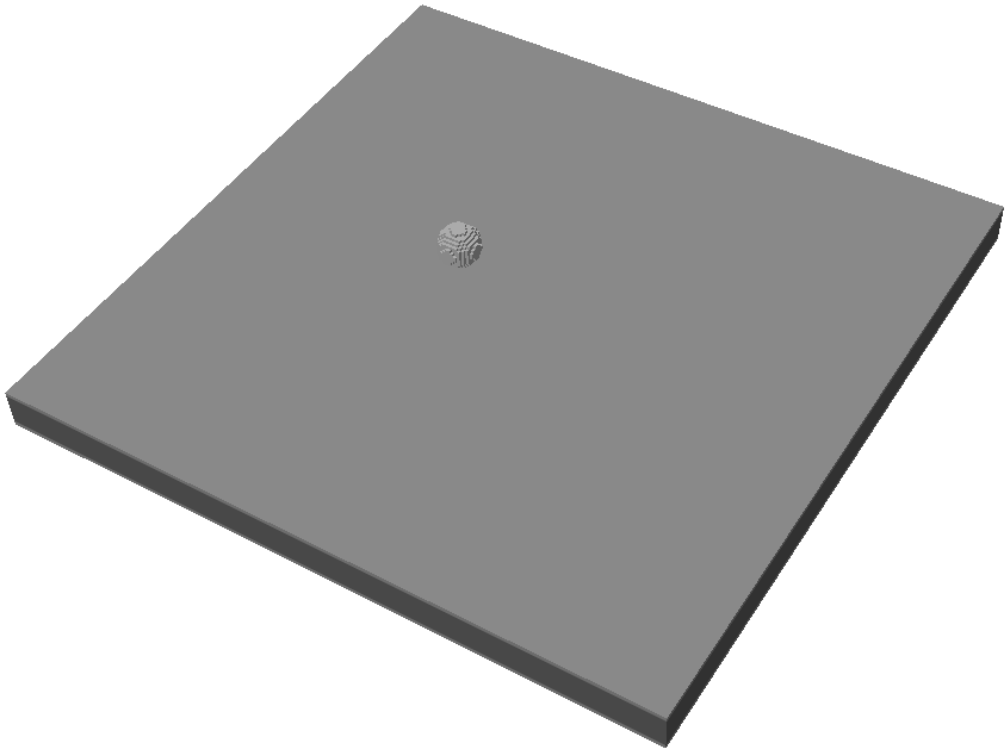

Figure 1. Initial configuration, simulation of NASA JSC experiment B1028.

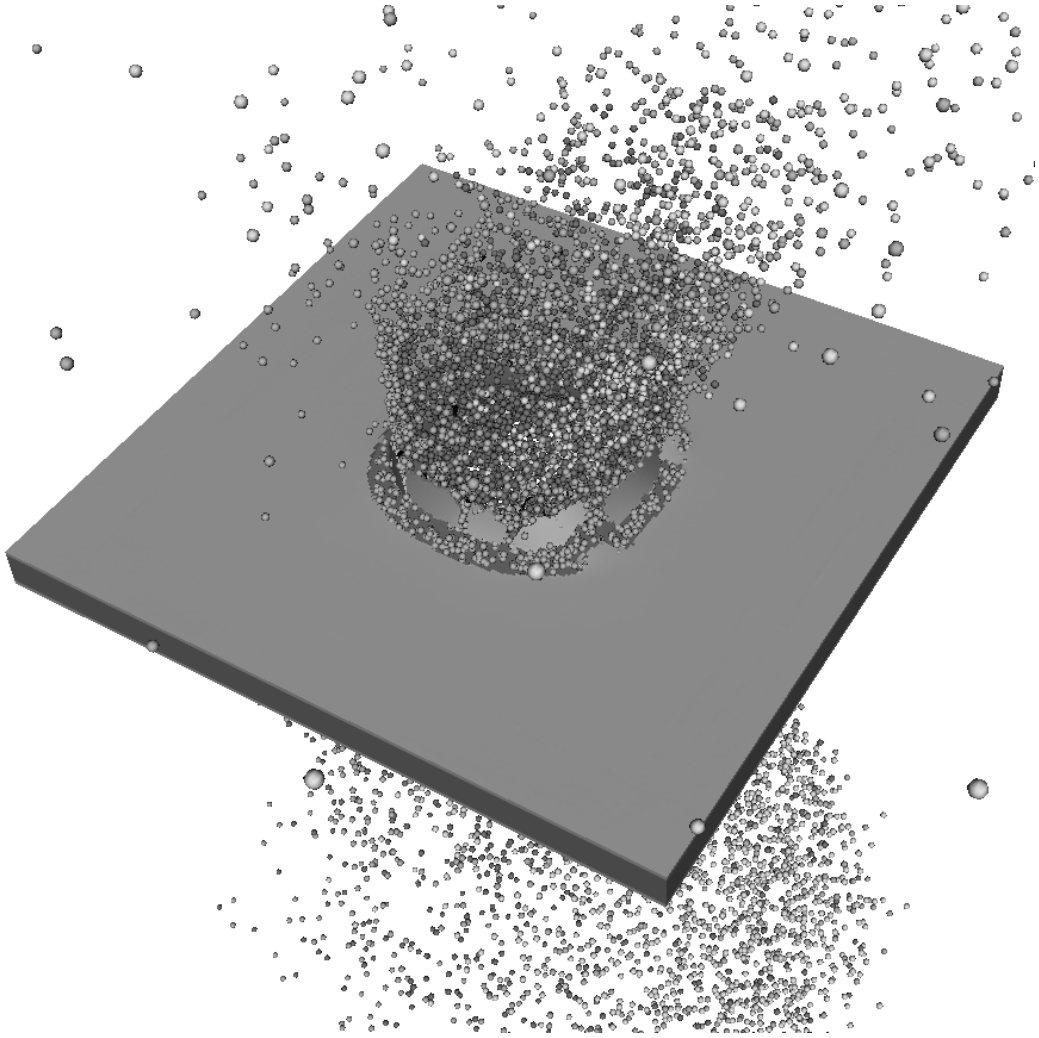

Figure 2. Particle-element plot of the simulation results at 50 microseconds after impact.

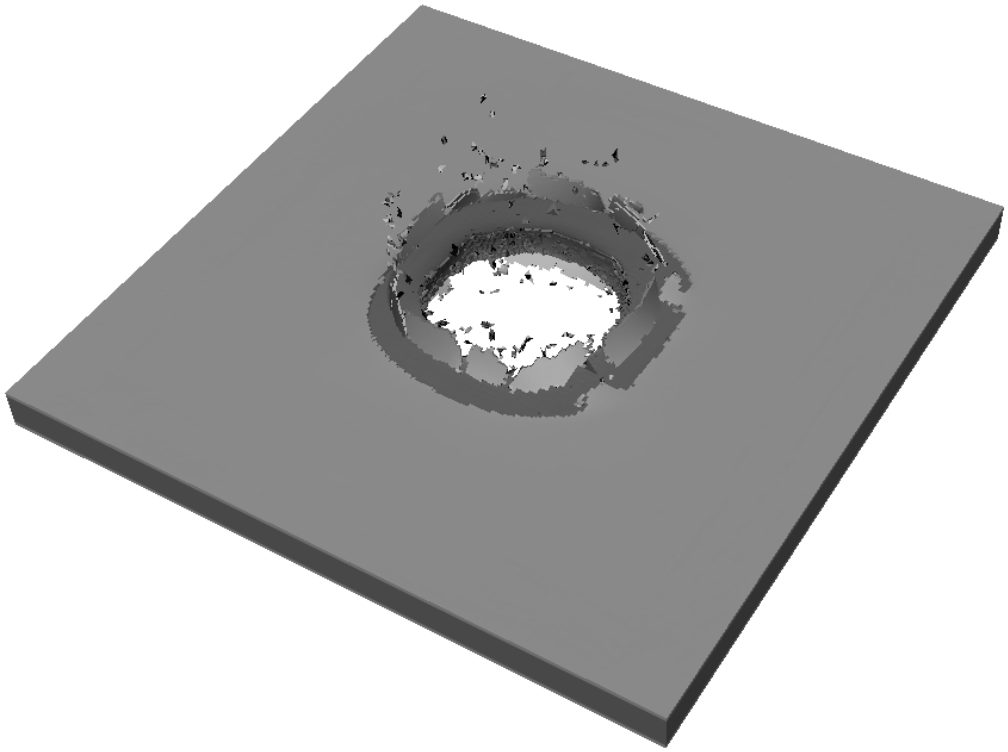

Figure 3. Element plot of the simulation results at 50 microseconds after impact.

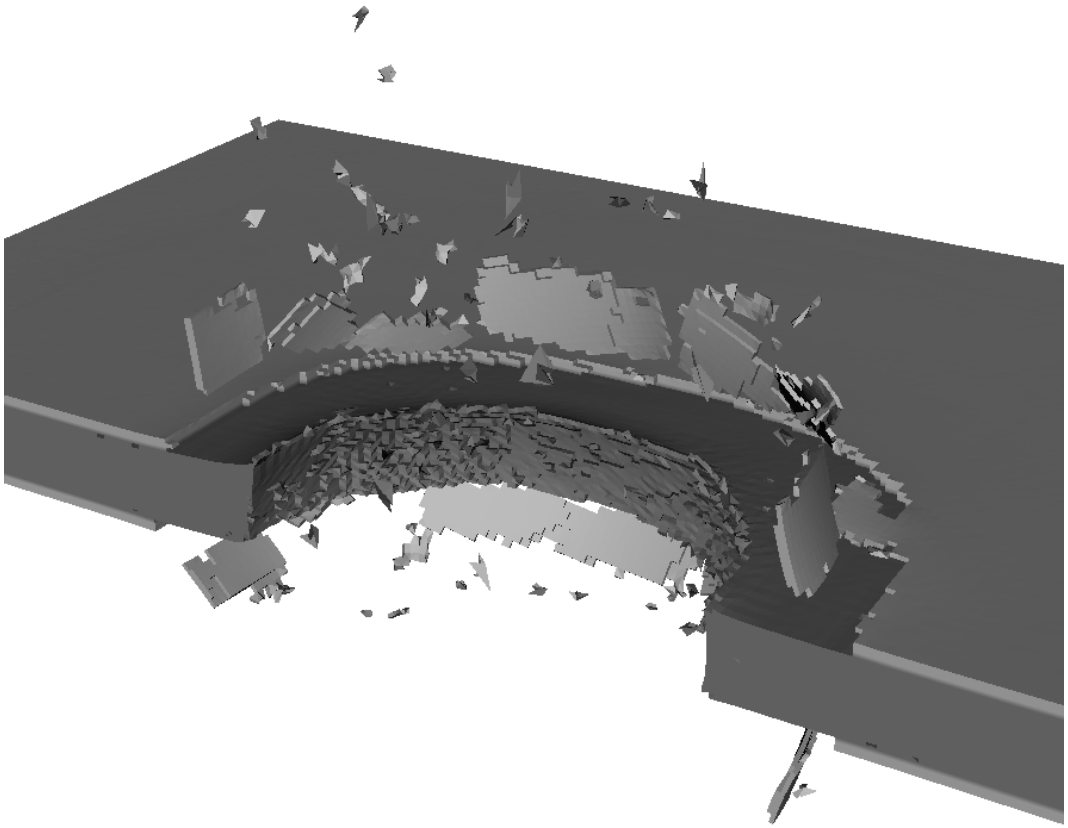

Figure 4. Sectioned element plot of the simulation results at 50 microseconds after impact.

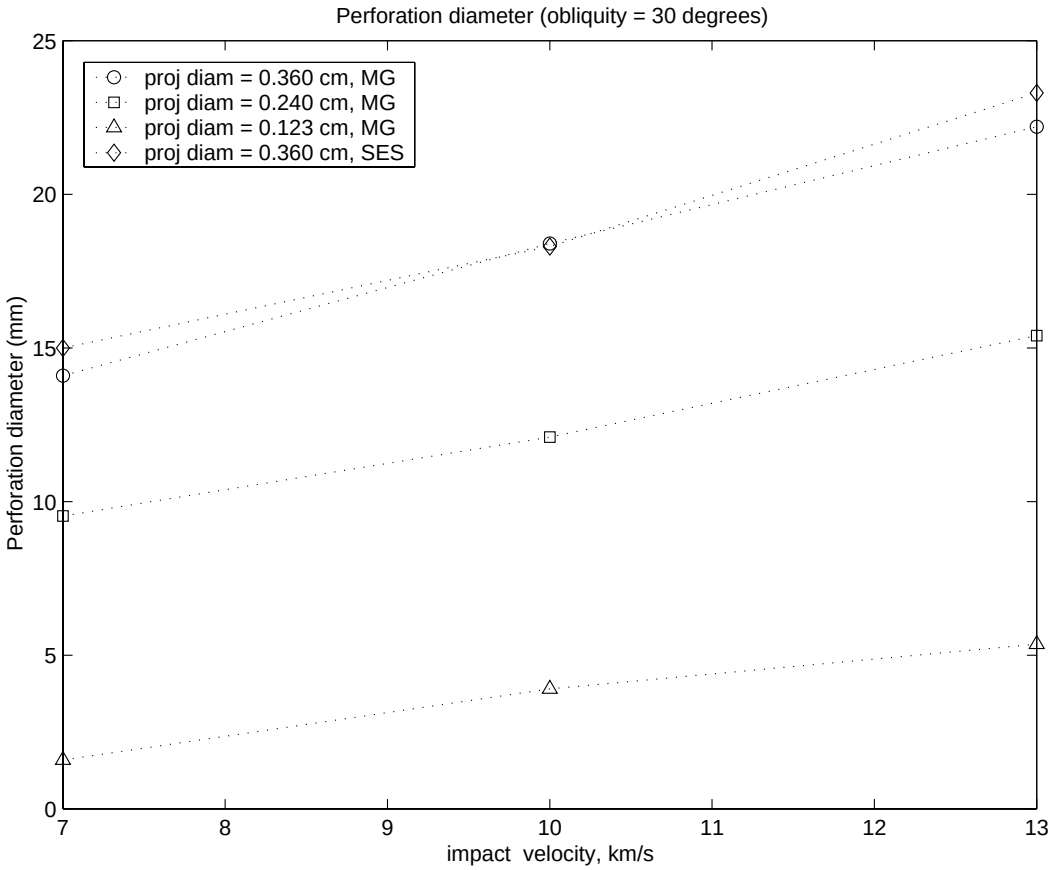

Figure 5. Simulation results for perforation diameter versus impact velocity.

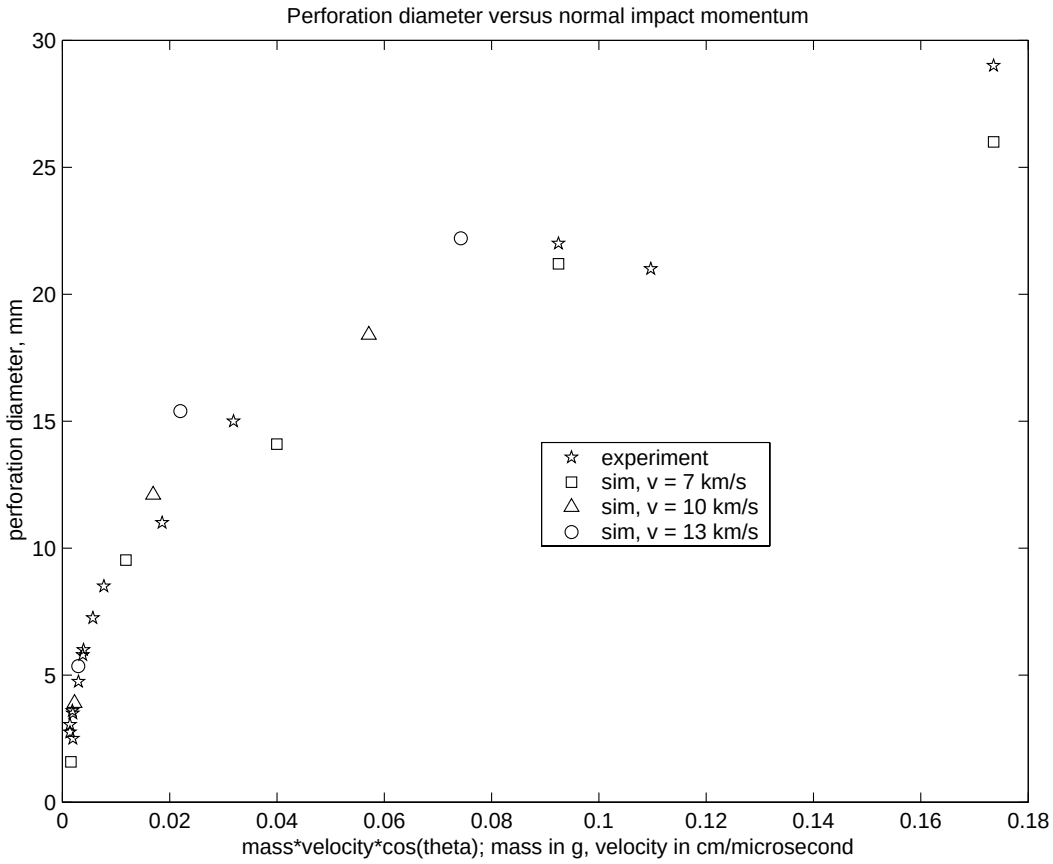

Figure 6. Perforation diameter versus normal impact momentum, for hypervelocity impact in reinforced carbon-carbon.